Taylor & Francis
Taylor & Francis Group

ORIGINAL RESEARCH

OPEN ACCESS | Check for updates

Spatial heterogeneity of immune infiltration predicts the prognosis of nasopharyngeal carcinoma patients

Ya-Qin Wang[a],[*], Xu Liu[a],[*], Cheng Xu[a],[*], Wei Jiang[b], Shuo-Yu Xu[a], Yu Zhang[a], Ye Lin Liang[a], Jun-Yan Li[a], Qian Li[a], Yu-Pei Chen[a], Yin Zhao[a], Jing-Ping Yun[a], Na Liu[a], Ying-Qin Li[a], and Jun Ma[a]

[a]State Key Laboratory of Oncology in South China, Collaborative Innovation Center of Cancer Medicine, Guangdong Key Laboratory of Nasopharyngeal Carcinoma Diagnosis and Therapy, Sun Yat-sen University Cancer Center, Guangzhou, P.R, China; [b]Department of Radiation Oncology, Guilin Medical University Affiliated Hospital, Guilin, China

ABSTRACT

Spatial information on the tumor immune microenvironment is of clinical relevance. Here, we aimed to quantify the spatial heterogeneity of lymphocytes and cancer cells and evaluated its prognostic value in patients with nasopharyngeal carcinoma (NPC). The scanned immunohistochemistry images of 336 NPC patients from two different hospitals were used to generate cell density maps for tumor and immune cells. Then, Getis-Ord hotspot analysis, a spatial statistic method used to describe species biodiversity in ecological habitats, was applied to identify cancer, immune, and immune-cancer hotspots. The results showed that cancer hotspots were not associated with any of the studied clinical outcomes, while immune-cancer hotspots predicted worse overall survival (OS) in the training cohort. In contrast, a high immune hotspot score was significantly associated with better OS (HR 0.41, 95% CI 0.22–0.77, P = .006), disease-free survival (DFS) (HR 0.43, 95% CI 0.24–0.75, P = .003) and distant metastasis-free survival (DMFS) (HR 0.40, 95% CI 0.20–0.81, P = .011) in NPC patients in the training cohort, and similar associations were also evident in the validation cohort. Importantly, multivariate analysis revealed that the immune hotspot score remained an independent prognostic indicator for OS, DFS, and DMFS in both cohorts. We explored the spatial heterogeneity of cancer cells and lymphocytes in the tumor microenvironment of NPC patients using digital pathology and ecological analysis methods and further constructed three spatial scores. Our study demonstrates that spatial variation may aid in the identification of the clinical prognosis of NPC patients, but further investigation is needed.

Introduction

Nasopharyngeal carcinoma (NPC) is a unique subtype of head and neck cancer with an unbalanced geographical distribution, demonstrating high prevalence in southern China, Southeast Asia, and North Africa.[1,2] Currently, the tumor-node-metastasis (TNM) staging system is the main tool for guiding treatment and predicting the prognosis of NPC. However, this system only takes anatomical data into consideration and provides insufficient prognostic information.[3] Pathologically, NPC is characterized by heavy infiltration of immune cells within and around tumor lesions and a high expression of PD-L1 or other immune checkpoints by both tumor and immune cells,[4–6] suggesting the existence of a complex tumor microenvironment (TME) in NPC. Therefore, TME-based biomarkers that reflect individual levels of immune heterogeneity are expected to predict the prognosis of NPC patients.

Pathology images of tumor tissues contain not only essential information for tumor histopathologic classification but also information on the TME, such as the spatial distribution of different types of cells.[7–9] Recently, with the development of computer vision techniques, digital pathology has emerged as a method enabling the automated identification and classification of various cell types and tumor regions, offering an opportunity to study the spatial heterogeneity and interactions between tumor and immune cells.[10,11] Important studies have found that the spatial interactions among tumor-infiltrating lymphocytes (TILs) and cancer cells generate complex ecological dynamics that can ultimately impact tumor progression and the response to treatment.[10,12] In addition, the spatial locations of cancer cells and immune cells have been shown to be associated with the clinical outcome of breast[13,14] and colorectal cancer.[15,16] Therefore, there is benefit in mapping the spatial distribution of cancer cells and lymphocytes using digital pathology and further evaluating its prognostic value for NPC patents.

In this study, we detected and quantified the spatial regions where the population of cancer cells or lymphocytes is significantly high, that is, cancer hotspots, immune hotspots, and immune-cancer hotspots, for NPC patients using deep learning. Furthermore, we evaluated the prognostic value of these three spatial hotspots and found that immune hotspots could stratify NPC patients with different risks. This is the first study

*Ya-Qin Wang, Xu Liu, and Cheng Xu contributed equally to this work.

Supplemental data for this article can be accessed on the publisher's website.

to highlight the important role of lymphocytes in predicting the prognosis of NPC patients from the perspective of spatial distribution.

Materials and methods

Clinical specimens

We retrospectively included 336 pretreatment, nonmetastatic NPC patients from two academic institutions in China. Of all specimens obtained for this study, 221 specimens obtained from the Sun Yat-sen University Cancer Center (Guangzhou) between January 2011 and December 2013 were designated as the training cohort, and 115 samples collected from the Affiliated Hospital of Guilin Medical University (Guilin) between November 2006 and October 2012 were used for validation. The American Joint Committee on Cancer (AJCC)-TNM Staging System Manual (8th Edition, 2017) was used to restage all patients.[3] This study was approved by the Institutional Ethical Review Boards of both hospitals, and all included patients gave informed consent before treatment. This study is reported according to the Reporting Recommendations for Tumor Marker Prognostic Studies (REMARK) criteria.[17]

Immunohistochemistry and digital pathology

First, slides were mounted with tumor sections obtained from paraffin-embedded tumor blocks; then, one slide for each patient was used for immunohistochemistry staining (IHC) with anti-CD3 (ab16669, 1:800; Abcam, Cambridge, UK). All slides were subsequently scanned, and the digital images were used for further analyses. The digital pathology techniques consisted of nucleus segmentation and tumor cell (TC) and immune cell (IC) population classification as described in our previous study.[5] Briefly, following stain deconvolution of the digital images, nucleus segmentation was performed in the hematoxylin channel using a regional convolutional neural network (R-CNN). Next, we classified the cells into TCs or ICs using the Xception deep learning model, which was developed based on the manual annotation of each nucleus as belonging to a TC or IC by two pathologists and achieved good performance (Supplementary Fig. S1).

Automated evaluation of spatial cancer, immune or immune-cancer hotspots

The centroid of each segmented nucleus was recognized as the cell location and was used to generate a cell density map for TCs and ICs. To characterize the spatial distributions of TCs and ICs, we adopted the Getis-Ord statistics-based approach[13,18] to identify cancer and immune hotspots, which are defined as areas of highly clustered tumor cells and lymphocytes, respectively. Specifically, each cell density map was processed within a set of 64 μm * 64 μm (128 pixels by 128 pixels) sliding windows to count the number of nuclei in each window. The z-score for each window was calculated based on the Getis-Ord local statistic, which takes into account the number of nuclei in the current window as well as in the corresponding first-, second- and third-order neighboring

windows. We used $P = .05$ and its associated z-score as the threshold, and all windows with larger z-scores were identified as significant spatial hotspots. After the cancer and immune hotspots were created, a colocalized hotspot (the immune-cancer hotspot) was also generated from the regions of overlap between the cancer hotspot and the immune hotspot (Figure 1). The spatial scores of the cancer hotspots, immune hotspots, and immune-cancer hotspots were calculated by quantifying the area percentage of each type of hotspot in the entire tissue (Supplementary Table S1–S2).

DNA extraction and real-time quantitative polymerase chain reaction

Plasma Epstein-Barr virus (EBV) DNA titers were routinely measured by real-time quantitative polymerase chain reaction assay before treatment for the NPC patients in the training cohort.[19] The pretreatment plasma EBV DNA titer cutoff value (2000 copies/mL) had been previously estimated to define low and high EBV DNA levels.[20]

Statistical analysis

In our study, overall survival (OS) was set as the primary endpoint, and the secondary endpoints were disease-free survival (DFS) and distant metastasis-free survival (DMFS). OS was calculated from the date of treatment to the date of death from any cause or the last date known alive. DFS was calculated from the first day of treatment to failure, death or the last visit, and DMFS was estimated from the first day of treatment to the first distant metastatic relapse.

The χ^2 test or Fisher's exact test was employed to analyze the associations between the immune hotspots and clinicopathological variables. Survival outcomes, namely, OS, DFS, and DMFS, were estimated by the Kaplan–Meier method and compared by the log-rank test. Multivariate analysis using a Cox proportional hazards model was performed to test for independent significance by backward selection. Hazard ratios (HRs) and 95% confidence intervals (CIs) were calculated using the Cox proportional hazards model. Variables with $P \leq 0.05$ were included in the multivariate analysis, and only independent prognostic factors were retained in the multivariate model.

All statistical tests were two-sided and considered significant when the P value was less than 0.05. Statistical analyses were performed using Statistical Package for the Social Sciences (SPSS) version 22.0 (IBM, Armonk, NY, USA). The key raw data have been uploaded to the Research Data Deposit public platform (www.researchdata.org.cn) with approval number RDDB2021000979.

Results

Correlations among infiltrating lymphocytes and spatial scores

The spatial patterns of TILs and cancer cells can be indicative of immune functional phenotypes and disease prognosis. Here, we analyzed the spatial heterogeneity of the tumor immune microenvironment of NPC patients using slides from our
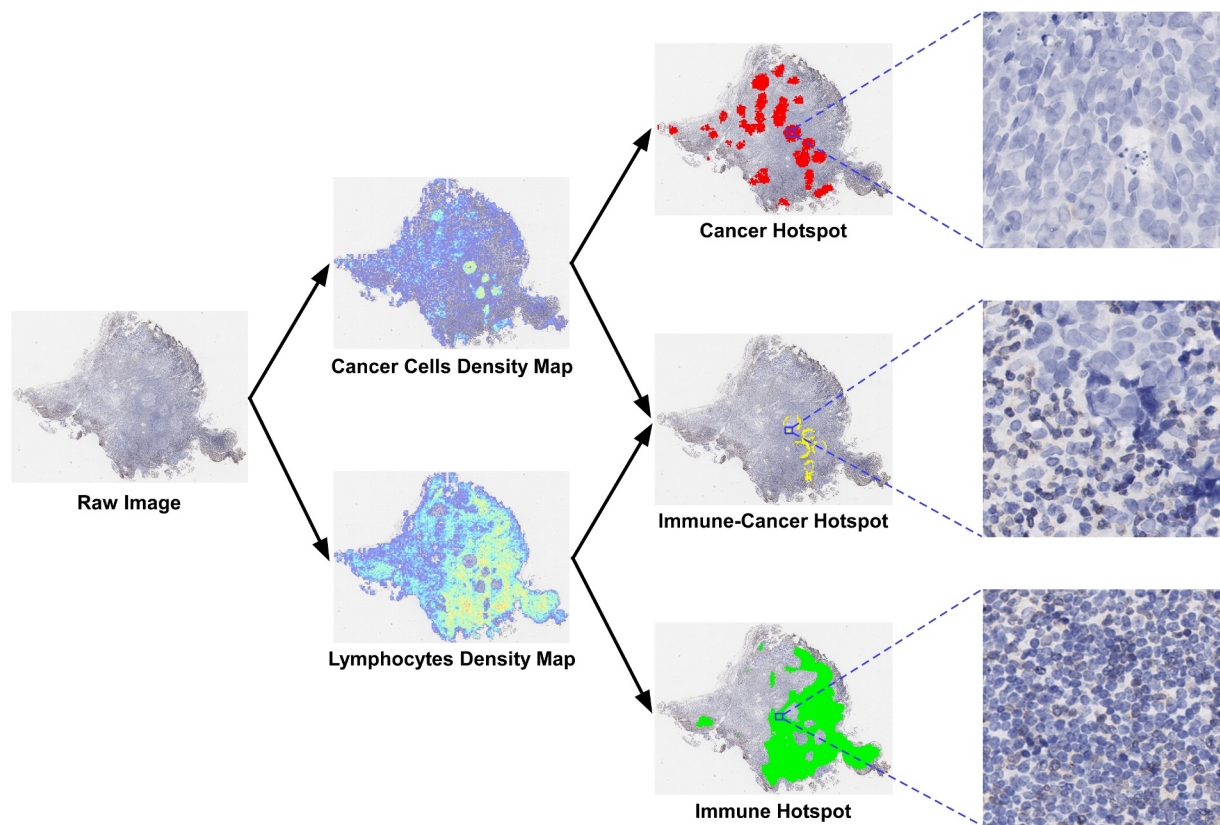
Figure 1. Illustration of the pipeline for identifying cancer hotspots, immune hotspots, and immune-cancer hotspots.

previous study.[21] Based on the whole-slide images, cancer hotspots, immune hotspots, and immune-cancer hotspots were identified, and three spatial scores were calculated using hotspot analysis (Getis-Ord spatial analysis). The clinicopathologic characteristics of the Guangzhou training cohort (n = 221) and the Guilin external validation cohort (n = 115) are summarized in Table 1. The median follow-up time was 69.7 months (interquartile range (IQR) 65.1–72.8) for the patients from the training cohort and 58 months (IQR 41–69) for those from the validation cohort.

The immune infiltrate densities of CD3, CD8, and CD45RO in the tumor and stromal areas and the corresponding immune scores (ISs) of these two cohorts were obtained in our previous study.[16] There was a strong, positive correlation between the IS and the infiltrate densities of CD3, CD8, and CD45RO in the tumor and stroma in the training cohort (r = 0.426–0.752) and validation cohort (r = 0.407–0.654), which is consistent with the definition of the immune score. Then, we investigated the correlations among the spatial scores; those among the spatial scores were weak in both the training cohort (|r| ≤ 0.069) and the validation cohort (|r| ≤ 0.175), suggesting the typical lack of tumor cell and lymphocyte clustering in NPC patients. Interestingly, in the training cohort, the immune hotspot was positively associated with infiltrating lymphocytes and the IS (r = 0.292–0.528), whereas the cancer hotspot was weakly negatively associated with lymphocytes and the IS (r < 0). These findings were confirmed in the validation cohort (Table 2).

Prognostic value of the spatial scores

Then, we explored the prognostic value of the cancer hotspots, immune hotspots, and immune-cancer hotspots in the training cohort. X-tile software was used to generate the optimal cutoff values for separating high and low spatial scores for the three hotspots, yielding values of 0.150 for the cancer hotspot score, 0.198 for the immune hotspot score, and 0.0045 for the immune-cancer hotspot score. Patients with a high immune hotspot score had a lower risk for death than patients with a low immune hotspot score (HR 0.41, 95% CI 0.22–0.77, P = .006, Figure 2a). However, a high immune-cancer hotspot score was associated with poorer OS than a low immune-cancer hotspot score (HR 1.98, 95% CI 1.04–3.78, P = .038, Figure 3a). Moreover, when patients were stratified by the spatial location of cancer cells, there were no significant differences in OS between the two groups in the training cohort (HR 1.66, 95% CI 0.81–3.41, P = .17, Figure 3a).

Further analysis demonstrated that in the training cohort, the presence of a high immune hotspot score was also associated with improved DFS (82.7% vs. 64.4%, HR 0.43, 95% CI 0.24–0.75, P = .003, Figure 2b) and DMFS (89.5% vs. 76.3%, HR 0.40, 95% CI 0.20–0.81, P = .011, Figure 2c). However, neither cancer hotspots nor immune-cancer hotspots showed an association with DFS or DMFS (Figure 3(b-C)).

To validate whether immune hotspots had similar prognostic value in different populations, we stratified the patients from the Guilin cohort into high immune hotspot (n = 63)

Table 1. Clinicopathological characteristics of the patients in the training and validation cohorts stratified by immune hotspot.

	All	Training cohort (n = 221)			Validation cohort (n = 115)		
		Low	High	P	Low	High	P
Total population	336 (100)	68 (30.8)	153 (69.2)		49 (42.6)	66 (57.4)	
Age				0.93			0.074
≤ 45 years	163 (48.5)	31 (52.5)	84 (51.9)		17 (32.7)	31 (49.2)	
> 45 years	173 (51.5)	28 (47.5)	78 (48.1)		35 (67.3)	32 (50.8)	
Sex				0.81			0.063
Male	254 (75.6)	45 (76.3)	121 (74.7)		44 (84.6)	44 (69.8)	
Female	82 (24.4)	14 (23.7)	41 (25.3)		8 (15.4)	19 (30.2)	
WHO pathological type				0.87			1.00
I/II	8 (2.4)	2 (3.4)	3 (1.9)		1 (1.9)	2 (3.2)	
III	328 (97.6)	57 (96.6)	159 (98.1)		51 (98.1)	61 (96.8)	
T Stage				0.15			**0.033**
T1-T2	136 (40.5)	16 (27.1)	61 (37.7)		21 (40.4)	38 (60.3)	
T3-T4	200 (59.5)	43 (72.9)	101 (62.3)		31 (59.6)	25 (39.7)	
N Stage				0.76			0.58
N0-N1	200 (59.5)	41 (69.5)	116 (71.6)		18 (34.6)	25 (39.7)	
N2-N3	136 (40.5)	18 (30.5)	46 (28.4)		34 (65.4)	38 (60.3)	
TNM Stage				0.34			0.076
I–II	87 (25.9)	14 (23.7)	51 (30.2)		8 (15.4)	16 (25.4)	
III–IV	249 (74.1)	45 (76.3)	113 (69.8)		44 (84.6)	47 (74.6)	
EBV-DNA load (copy/mL)				0.90			NA
≤ 2000	122 (55.2)	33 (55.9)	89 (54.9)		NA	NA	
> 2000	99 (44.8)	26 (44.1)	73 (45.1)		NA	NA	
Death				**0.009**			**0.003**
Yes	74 (22.0)	17 (28.8)	22 (13.6)		23 (44.2)	12 (19.0)	
No	262 (78.0)	42 (71.2)	140 (86.4)		29 (55.8)	51 (81.0)	
Distant metastasis				**0.012**			**0.01**
Yes	56 (16.7)	14 (23.7)	17 (10.5)		17 (32.7)	8 (12.7)	
No	280 (83.3)	45 (76.3)	145 (89.5)		35 (67.3)	55 (87.3)	
Locoregional failure				0.11			0.70
Yes	51 (15.2)	9 (15.3)	13 (8.0)		14 (26.9)	15 (23.8)	
No	285 (84.8)	50 (84.7)	149 (92.0)		38 (73.1)	48 (76.2)	
Disease progression				**0.004**			**0.011**
Yes	94 (28.0)	21 (35.6)	28 (17.3)		27 (51.9)	18 (28.6)	
No	242 (72.0)	38 (64.4)	134 (82.7)		25 (48.1)	45 (71.4)	

Abbreviations: TNM, Tumor-node-metastasis; EBV-DNA, Epstein-Barr virus DNA.

Table 2. The correlation between three spatial hotspots, infiltrating lymphocytes and immune score in the training and validation cohorts (r value are presented; *P < .05, **P < .01).

Variable	Cancer Hotspot	Immune Hotspot	Immune-Cancer Hotspot	I-CD3	S-CD3	I-CD8	S-CD8	I-CD45RO	S-CD45RO	IS
Training cohort										
Cancer Hotspot	–	–	–	–	–	–	–	–	–	–
Immune Hotspot	−0.029	–	–	–	–	–	–	–	–	–
Immune-Cancer Hotspot	−0.059	0.069	–	–	–	–	–	–	–	–
I-CD3	−0.107	0.367**	0.186**	–	–	–	–	–	–	–
S-CD3	−0.225**	0.318**	0.156*	0.341**	–	–	–	–	–	–
I-CD8	−0.122	0.446**	0.146*	0.457**	0.350**	–	–	–	–	–
S-CD8	−0.124	0.455**	0.092	0.233**	0.418**	0.545**	–	–	–	–
I-CD45RO	−0.08	0.299**	0.085	0.390**	0.264**	0.440**	0.304**	–	–	–
S-CD45RO	−0.133*	0.292**	0.067	0.239**	0.359**	0.384**	0.504**	0.541**	–	–
IS	−0.176**	0.528**	0.140*	0.565**	0.426**	0.752**	0.589**	0.679**	0.534**	–
Validation cohort										
Cancer Hotspot	–	–	–	–	–	–	–	–	–	–
Immune Hotspot	−0.175	–	–	–	–	–	–	–	–	–
Immune-Cancer Hotspot	0.042	−0.029	–	–	–	–	–	–	–	–
I-CD3	−0.123	0.174	0.089	–	–	–	–	–	–	–
S-CD3	−0.285**	0.429**	0.024	0.422**	–	–	–	–	–	–
I-CD8	−0.162	0.567**	0.110	0.285**	0.339**	–	–	–	–	–
S-CD8	−0.182	0.544**	−0.049	0.241*	0.483**	0.467**	–	–	–	–
I-CD45RO	−0.124	0.313**	0.096	0.011	0.115	0.399**	0.231*	–	–	–
S-CD45RO	−0.135	0.507**	−0.009	0.137	0.340**	0.297**	0.582**	0.314**	–	–
IS	−0.240*	0.595**	0.028	0.470**	0.407**	0.646**	0.654**	0.430**	0.609**	–

and low immune hotspot (n = 52) groups using the cutoff value obtained for the training cohort. Survival analysis showed that patients with high immune hotspot scores also had longer OS (81.0% vs. 55.8%, HR 0.38, 95% CI 0.19–0.77, P = .007), DFS (71.4% vs. 48.1%, HR 0.48, 95% CI 0.27–0.88, P = .016) and DMFS times (87.3% vs. 67.3%, HR 0.34, 95% CI 0.15–0.79, P = .012, Figure 2(d-F)) than those with low immune hotspot scores.
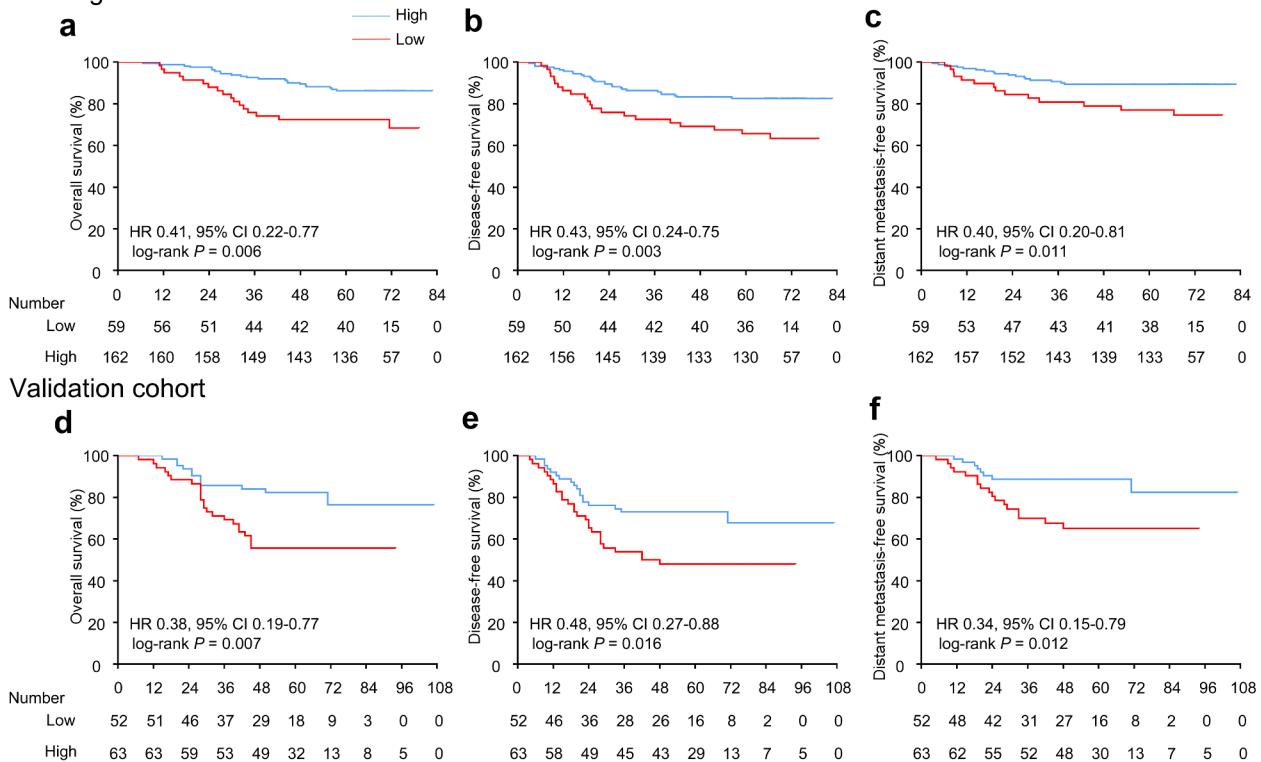
Training cohort

Figure 2. Kaplan–Meier curves of overall, disease-free and distant metastasis-free survival according to the spatial score of the immune hotspots identified in CD3⁺ immunohistochemistry slides in the training and validation cohorts. Plots show (a) overall survival, (b) disease-free survival and (c) distant metastasis-free survival in the training cohort and (d) overall survival, (e) disease-free survival and (f) distant metastasis-free survival in the validation cohort. Abbreviations: HR, hazard ratio; and CI, confidence interval.

Univariate analyses were performed in the training and validation cohorts, and the results showed that immune hotspot, TNM stage, and pretreatment EBV DNA levels were significantly associated with OS, DFS, and DMFS in the training cohort. Moreover, immune hotspot and TNM stage were also significantly associated with OS, DFS, and DMFS in the validation cohort (Figure 3). Then, we performed multivariate Cox regression analysis, after which immune hotspots remained significant for OS, DFS, and DMFS in the training cohort (OS: HR 0.40, 95% CI 0.21–0.76, P = .005; DFS: HR 0.42, 95% CI 0.24–0.74, P = .003; and DMFS: HR 0.39, 95% CI 0.19–0.80, P = .01) and validation cohort (OS: HR 0.42, 95% CI 0.21–0.84, P = .015; DFS: HR 0.52, 95% CI 0.29–0.94, P = .031; and DMFS: HR 0.37, 95% CI 0.16–0.86, P = .021). TNM stage and pretreatment EBV DNA levels were also significantly associated with OS, DFS, and DMFS in multivariate analysis (Table 3).

Discussion

In this study, we aimed to elucidate the spatial heterogeneity of tumor and immune cells and their spatial relationship using deep learning and further evaluated their prognostic value in two NPC patient cohorts. Our results showed that immune hotspots, which reflect the spatial distribution patterns of different immune cell subsets, are highly prognostic, whereas cancer hotspots and immune-cancer hotspots are not. To the best of our knowledge, this study was the first to evaluate and validate the prognostic significance of

spatial scores in NPC patients, highlighting the importance of examining not only immune cell density but also spatial patterns that can be indicative of immune status and disease prognosis.

Immune infiltration in the tumor immune microenvironment has attracted considerable attention for many years, and the prognostic value of the type and density of TILs has been extensively explored.[22–25] However, due to the complexity of the tumor microenvironment and the limited number of analytical methods, the spatial heterogeneity of TILs, which is a fundamental biological feature of the microenvironment, has been largely ignored. Recently, by applying principles and quantitative methods from ecology, Nawaz et al. identified cancer and immune hotspots in estrogen receptor-negative (ER-) breast cancer and further reported that the amount of colocalized cancer and immune hotspots weighted by the tumor area correlated with prognosis.[18] In addition, with the same methods, Heindl et al. demonstrated that immune hotspots based on the spatial heterogeneity of TILs were highly prognostic for late recurrence in patients with ER-positive (ER+) breast cancer after endocrine therapy.[13] Unfortunately, until now, little has been known about the spatial heterogeneity of cancer and immune cells in histological samples and its prognostic value in NPC patients. Here, for the first time, we determined cancer hotspots, immune hotspots, and immune-cancer hotspots in NPC patients and further investigated their influence on clinical outcomes.
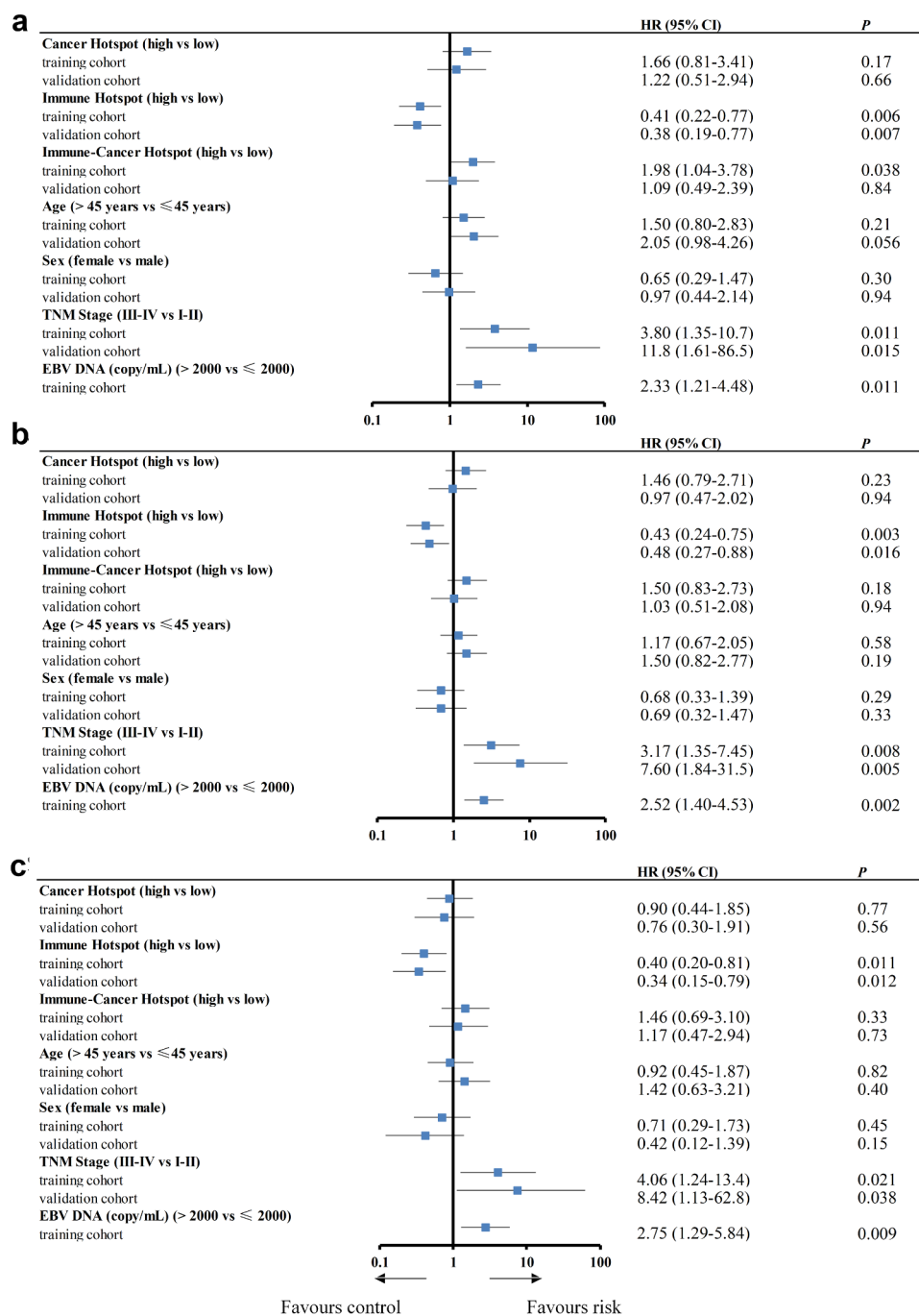
Figure 3. Univariate analysis of factors associated with overall survival, disease-free survival, and distant metastasis-free survival in the training and validation cohorts. Plots show (a) overall survival, (b) disease-free survival and (c) distant metastasis-free survival. Abbreviations: HR, hazard ratio; CI, confidence interval; TNM, tumor-node-metastasis EBV DNA; Epstein-Barr virus DNA.

Recent advances in cancer research have shown that tumors, like species striving for survival, harbor intricate population dynamics, which suggests the possibility of exploiting the evolution and ecology of tumors to understand the complex dynamics of the TME and predict clinical outcomes.[10] In ecological studies, the spatial distribution of species in their habitats is a key determinant in accessing resources, evading predators and interacting with other organisms and the environment.[26,27] Getis-Ord hotspot analysis, a spatial statistics method that has been widely used with ecological and demographic data to analyze spatial interactions, can pinpoint regions with statistically significant spatial clustering of high magnitudes of a particular variable.[13,28] Thus, with this method, we can map the spatial distribution of cancer cells and lymphocytes in the TME. In this study, applying deep learning, spatial statistics and ecological theory, we detected the spatial patterns of cancer cells and lymphocytes in NPC patients from two different hospitals and further evaluated their prognostic value in these two independent cohorts. Our results suggest that immune hotspots, but not cancer hotspots or immune-cancer hotspots, could predict the OS, DFS, and DMFS of NPC patients.

Table 3. Multivariable Cox regression analysis of factors associated with overall survival, disease-free survival, and distant metastasis-free survival in the training and validation cohorts.

Variable	Training cohort (n = 221)		Validation cohort (n = 115)	
	HR (95% CI)	P	HR (95% CI)	P
overall survival				
Immune Hotspot (high vs low)	0.40 (0.21–0.76)	**0.005**	0.42 (0.21–0.84)	**0.015**
TNM Stage (III–IV vs. I–II)	3.25 (1.15–9.20)	**0.026**	10.8 (1.46–79.2)	**0.020**
EBV-DNA (> 2000 vs.≤ 2000)	2.12 (1.09–4.09)	**0.026**	NA	NA
disease-free survival				
Immune Hotspot (high vs low)	0.42 (0.24–0.74)	**0.003**	0.52 (0.29–0.94)	**0.031**
TNM Stage (III–IV vs. I–II)	2.63 (1.11–6.21)	**0.028**	7.20 (1.73–29.9)	**0.007**
EBV-DNA (> 2000 vs.≤ 2000)	2.30 (1.27–4.16)	**0.006**	NA	NA
distant metastasis-free survival				
Immune Hotspot (high vs low)	0.39 (0.19–0.80)	**0.01**	0.37 (0.16–0.86)	**0.021**
TNM Stage (III–IV vs. I–II)	3.32 (1.00–11.0)	**0.049**	7.71 (1.03–57.9)	**0.047**
EBV-DNA (> 2000 vs.≤ 2000)	2.48 (1.16–5.29)	**0.019**	NA	NA

Abbreviations: HR, hazard ratio; CI, confidence interval; TNM, Tumor-node-metastasis; EBV-DNA, Epstein-Barr virus DNA.

Previously, we identified the IS of NPC based on the densities of different CD3, CD8 and CD45RO lymphocyte populations in the tumor and stroma using digital pathology, which can also provide prognostic information for NPC patients.[21] The IS provides information on the immune infiltration of different lymphocyte populations in the tumor immune microenvironment, which can help classify tumors into different categories and potentially represents a practical tool for directing therapeutic intervention.[29,30] This study provided an additional dimension to the analysis of the immune functional phenotype in NPC. Here, for the first time, we investigated the spatial distribution patterns of TILs and constructed three spatial hotspots for NPC patients, which provide effective approaches to explore the spatial heterogeneity and interaction between immune and cancer cells in NPC. In addition, our results show that immune hotspots could predict the prognosis of NPC patients, which confirmed the positive prognostic value of immune infiltration from the perspective of spatial distribution. Multivariate analysis showed that not only immune hotspots but also TNM stage were significantly associated with OS, DFS, and DMFS in both cohorts. Currently, TNM staging is the key determinant for prognostic prediction in NPC patients in routine clinical practice, which provides useful prognostic information and deserves further investigation.

Certain limitations in our study are worth mentioning. We selected a window size of 128 pixels*128 pixels to perform digital pathology according to evidence provided in a previous publication.[18] However, the prognostic significance of the hotspot scores might be sensitive to the window size adopted in the Getic-Ord analysis. Comprehensive comparisons between various window sizes should be performed in future, larger cohort studies.

In summary, we explored the spatial heterogeneity of neoplastic cells and immune cells in the TME of NPC patients using digital pathology and ecological analysis methods. Furthermore, three spatial scores were constructed, revealing that the immune hotspot was an independent prognostic factor for clinical outcomes in both the training and validation cohorts. The addition of spatial analysis to the evaluation of the types and abundance of immune cells in the TME with digital pathology may aid in the identification of relevant clinical prognosis and treatment selection features, all of which deserve further analysis.

Availability of data and materials

The datasets used and/or analysed during the current study are available from the corresponding author on reasonable request.

Disclosure statement

The author(s) declare that they have no conflicts of interest.

Abbreviations

NPC, nasopharyngeal carcinoma; OS, overall survival; DFS, disease-free survival; DMFS, distant metastasis-free survival; HR, hazard ratio; CI, confidence interval; TILs, tumour-infiltrating lymphocytes.

Author contributions

Conceptualization: Y.Q. Wang and J. Ma.
Data curation: Y.Q. Wang, L. X. Liu, C. Xu, and S.Y. Xu.
Formal analysis: Y.Q. Wang, X. Liu, C. Xu, W. Jiang, S.Y. Xu, Y. Zhang, Y.L. Liang, J.Y. Li, Q. Li, Y.P. Chen, Y. Zhao, J.P. Yun, N. Liu, and Y.Q. Li.
Funding acquisition: J. Ma.
Methodology: Y.Q. Wang, X. Liu, C. Xu, and Y. Zhang.
Project administration: Y.Q. Wang, J.P. Yun, N. Liu, Y.Q. Li, and J. Ma.
Supervision: J. Ma.
Roles/Writing - original draft: Y.Q. Wang, X. Liu, C. Xu, Y.Q. Li, and J. Ma.

Ethics approval and consent to participate

References

1. Chen Y-P, Chan ATC, Le Q-T, Blanchard P, Sun Y, Ma J. Nasopharyngeal carcinoma. The Lancet. 2019;394(10192):64–80. doi:10.1016/S0140-6736(19)30956-0.

2. Bray F, Ferlay J, Soerjomataram I, Siegel RL, Torre LA, Jemal A. Global cancer statistics 2018: GLOBOCAN estimates of incidence and mortality worldwide for 36 cancers in 185 countries. CA Cancer J Clin. 2018;68:394–424.

3. Amin MB. American Joint Committee on Cancer. AJCC cancer staging manual. 8th ed. New York (NY): Springer; 2017.

4. Wang YQ, Chen YP, Zhang Y, Jiang W, Liu N, Yun J-P, Sun Y, He Q-M, Tang X-R, Wen X, et al. Prognostic significance of tumor-infiltrating lymphocytes in nondisseminated nasopharyngeal carcinoma: a large-scale cohort study. Int J Cancer. 2018;142(12):2558–2566. doi:10.1002/ijc.31279.

5. Wang Y-Q, Zhang Y, Jiang W, Chen Y-P, Xu S-Y, Liu N, Zhao Y, Li L, Lei Y, Hong X-H, et al. Development and validation of an immune checkpoint-based signature to predict prognosis in nasopharyngeal carcinoma using computational pathology analysis. J ImmunoTher Cancer. 2019;7(1):298. doi:10.1186/s40425-019-0752-4.

6. Ono T, Azuma K, Kawahara A, Sasada T, Matsuo N, Kakuma T, Kamimura H, Maeda R, Hattori C, On K, et al. Prognostic stratification of patients with nasopharyngeal carcinoma based on tumor immune microenvironment. Head Neck. 2018;40(9):2007–2019. doi:10.1002/hed.25189.

7. Wang S, Rong R, Yang D, Fujimoto J, Yan S, Cai L, Yang L, Luo D, Behrens C, Parra ER, et al. Computational staining of pathology images to study the tumor microenvironment in lung cancer. Cancer Res. 2020;80(10):2056–2066. doi:10.1158/0008-5472.CAN-19-1629.

8. Travis W, Brambilla E, Nicholson A, Yatabe Y, Austin JHM, Beasley MB, Chirieac LR, Dacic S, Duhig E, Flieder DB, et al. The 2015 World Health Organization classification of lung tumors: impact of genetic, clinical and radiologic advances since the 2004 classification. J Thorac Oncol. 2015;10(9):1243–1260. doi:10.1097/JTO.0000000000000630.

9. Wang HY, Chang YL, To KF, Hwang JSG, Mai H-Q, Feng Y-F, Chang ET, Wang C-P, Kam MKM, Cheah S-L, et al. A new prognostic histopathologic classification of nasopharyngeal carcinoma. Chin J Cancer. 2016;35(1):41. doi:10.1186/s40880-016-0103-5.

10. Nawaz S, Yuan YY. Computational pathology: exploring the spatial dimension of tumor ecology. Cancer Lett. 2016;380(1):296–303. doi:10.1016/j.canlet.2015.11.018.

11. Nearchou I, Soutar D, Ueno H, Harrison D, Arandjelovic O, Caie P. A comparison of methods for studying the tumor microenvironment's spatial heterogeneity in digital pathology specimens. J Pathol Inform. 2021;12(1):6. doi:10.4103/jpi.jpi_26_20.

12. Yuan Y. Spatial Heterogeneity in the Tumor Microenvironment. Cold Spring Harbor perspectives in medicine; 20166(8):a026583.

13. Heindl A, Sestak I, Naidoo K, Cuzick J, Dowsett M, Yuan Y. Relevance of spatial heterogeneity of immune infiltration for predicting risk of recurrence after endocrine therapy of ER+ breast cancer. JNCI: Journal of the National Cancer Institute. 2018;110(2):2. doi:10.1093/jnci/djx137.

14. Maley C, Koelble K, Natrajan R, Aktipis A, Yuan Y. An ecological measure of immune-cancer colocalization as a prognostic factor for breast cancer. Breast Cancer Res. 2015;17(1):131. doi:10.1186/s13058-015-0638-4.

15. Nearchou I, Gwyther B, Georgiakakis E, Gavriel CG, Lillard K, Kajiwara Y, Ueno H, Harrison DJ, Caie PD. Spatial immune profiling of the colorectal tumor microenvironment predicts good outcome in stage II patients. Npj Digital Med. 2020;3(1):1. doi:10.1038/s41746-020-0275-x.

16. Rasmusson A, Zilenaite D, Nestarenkaite A, Augulis R, Laurinaviciene A, Ostapenko V, Poskus T, Laurinavicius A. Immunogradient indicators for antitumor response assessment by automated tumor-stroma interface zone detection. Am J Pathol. 2020;190(6):1309–1322. doi:10.1016/j.ajpath.2020.01.018.

17. McShane LM, Altman DG, Sauerbrei W, Taube SE, Gion M, Clark GM. Reporting recommendations for tumor marker prognostic studies (REMARK). J Natl Cancer Inst. 2005;97(16):1180–1184. doi:10.1093/jnci/dji237.

18. Nawaz S, Heindl A, Koelble K, Yuan Y. Beyond immune density: critical role of spatial heterogeneity in estrogen receptor-negative breast cancer. Mod Pathol. 2015;28(6):766–777. doi:10.1038/modpathol.2015.37.

19. Shao J-Y, Li Y-H, Gao H-Y, Wu Q-L, Cui N-J, Zhang L, Cheng G, Hu L-F, Ernberg I, Zeng Y-X, et al. Comparison of plasma Epstein–Barr virus(EBV) DNA levels and serum EBV immunoglobulin A/virus capsid antigen antibody titers in patients with nasopharyngeal carcinoma. Cancer. 2004;100(6):1162–1170. doi:10.1002/cncr.20099.

20. Guo R, Tang LL, Mao YP, Du X-J, Chen L, Zhang Z-C, Liu L-Z, Tian L, Luo X-T, Xie Y-B, et al. Proposed modifications and incorporation of plasma Epstein-Barr virus DNA improve the TNM staging system for Epstein-Barr virus-related nasopharyngeal carcinoma. Cancer. 2019;125(1):79–89. doi:10.1002/cncr.31741.

21. Wang Y, Chen L, Mao Y, Li YQ, Jiang W, Xu SY, Zhang Y, Chen YP, Li XM, He QM, et al. Prognostic value of immune score in nasopharyngeal carcinoma using digital pathology. J ImmunoTher Cancer. 2020;8:2.

22. Gabrielson A, Wu Y, Wang H, Jiang J, Kallakury B, Gatalica Z, Reddy S, Kleiner D, Fishbein T, Johnson L, et al. Intratumoral CD3 and CD8 T-cell densities associated with relapse-free survival in HCC. Cancer Immunol Res. 2016;4:419–430.

23. Wen T, Wang Z, Li Y, Li Z, Che X, Fan Y, Wang S, Qu J, Yang X, Hou K, et al. A four-factor immunoscore system that predicts clinical outcome for stage II/III gastric cancer. Cancer Immunol Res. 2017;5:524–534.

24. Pagès F, Mlecnik B, Marliot F, Bindea G, Ou FS, Bifulco C, Lugli A, Zlobec I, Rau TT, Berger MD, et al. International validation of the consensus Immunoscore for the classification of colon cancer: a prognostic and accuracy study. Lancet. 2018;391:2128–2139.

25. Okadome K, Baba Y, Yagi T, Kiyozumi Y, Ishimoto T, Iwatsuki M, Miyamoto Y, Yoshida N, Watanabe M, Baba H. Prognostic nutritional index, tumor-infiltrating lymphocytes, and prognosis in patients with esophageal cancer. Ann Surg. 2020;271:693–700.

26. Axelrod R, Axelrod DE, Pienta KJ. Evolution of cooperation among tumor cells. Proc Natl Acad Sci U S A. 2006;103(36):13474–13479. doi:10.1073/pnas.0606053103.

27. Cosner C, DeAngelis D, Ault J, Olson D. Effects of spatial grouping on the functional response of predators. Theor Popul Biol. 1999;56(1):65–75. doi:10.1006/tpbi.1999.1414.

28. Getis A, Ord JK. The Analysis of Spatial Association by Use of Distance Statistics. 2010;24(3).

29. Galon J, Bruni D. Approaches to treat immune hot, altered and cold tumors with combination immunotherapies. Nat Rev Drug Discov. 2019;18:197–218.

30. Angell HK, Bruni D, Barrett JC, Herbst R, Galon J. The Immunoscore: colon Cancer and Beyond. Clin Cancer Res. 2020;26(2):332–339. doi:10.1158/1078-0432.CCR-18-1851.